RSC Advances




ROYAL SOCIETY OF CHEMISTRY

www.rsc.org/advances

# Preparation and characterization of $TiO_2$ and $\gamma$-$Al_2O_3$ composite membranes for the separation of oil-in-water emulsions

**Kanchapogu Suresh, Tekula Srinu, Aloke Kumar Ghoshal and G. Pugazhenthi***

Department of Chemical Engineering, Indian Institute of Technology Guwahati, Guwahati-781039, Assam, India.

* To whom correspondence should be addressed.

Email: pugal@iitg.ernet.in (G. Pugazhenthi),

Telephone: 91-361-2582264,

Fax: 91 361-2582291.

## Abstract

Clay based ceramic support was prepared by uniaxial pressing method and Titanium dioxide ($TiO_2$) and γ-Alumina (γ-$Al_2O_3$) composite membranes were fabricated individually by coating of $TiO_2$ and γ-$Al_2O_3$ particles on the prepared ceramic support via hydrothermal method. The prepared $TiO_2$ and γ-$Al_2O_3$ powders as well as membranes were systematically characterized using analytical techniques such as thermogravimetric analysis (TGA), Fourier transform infrared spectroscopy (FTIR), BET surface area, X-ray diffraction analysis (XRD), particle size analyzer, scanning electron microscope (SEM), porosity, field emission scanning electron microscope (FESEM), $N_2$ gas permeation and pure water permeability. Filtration experiments were performed to evaluate the performance of the support and membranes by separation of synthetic oil-in-water emulsions. The effects of applied pressure and feed (oil) concentration on the treatment of oil-in-water emulsion for the support and membranes were examined. $TiO_2$ membrane demonstrates better rejection (97-99 %) and permeate flux (8.48-55.13×$10^{-5}$ $m^3/m^2s$) as compared to the support (rejection of 95-97 % and permeate flux of 1.87-9.84×$10^{-5}$ $m^3/m^2s$). Also the γ-$Al_2O_3$ membrane shows good rejection (96-98 %) and permeate flux (6.12-22.03×$10^{-5}$ $m^3/m^2s$). Despite similar rejection shown by the support and composite membranes, the flux of the $TiO_2$ membrane is one order higher than that of the support due to the enhanced hydrophilic character of the membrane after $TiO_2$ coating. Hence, the prepared composite membranes can be used as potential candidates for the treatment of oil-in-water emulsions.


Key words: Clay support, Composite membrane, Porosity, Water flux, Oil-in-water emulsions

## 1. Introduction

Several industries, including petrochemical, metallurgical, food processing, transportation and petroleum, generate a large quantity of oily wastewater emulsions.[1-4] This oily wastewater needs to be treated before discharging into the environment. Conventional treatment methods (incineration, gravity settling, dewatering, clarification and chemical treatment) have many disadvantages such as low efficiency, complex operational procedures and chemical contamination of effluents.[5-8] In recent years, membrane technology has been considered as a most effective, economical and environmentally friendly process for the filtration of oil polluted water due to its compact design and simple operating procedure. In membrane technology, polymeric and ceramic membranes have been applied for the separation of oil polluted water. Membranes made by inorganic materials have several advantages, including superior thermal, chemical and mechanical stability. Ceramic membranes prepared from $Al_2O_3$, $ZrO_2$, $SiO_2$ and $TiO_2$ are expensive due to the high cost of raw materials used for the synthesis as well as high sintering temperatures.[9-17]

Therefore, recently, researchers focused towards the fabrication of ceramic membranes using low-priced clays and utilized these membranes for the removal of oil from oil-in-water emulsion.[18] Few of the studies revealed that the surface character of the membrane plays an important role in separation of oil-water emulsions.[19-21] In particular, the hydrophilic membranes reduce the fouling by minimizing the formation of the cake layer on the surface.[19,21] Prior to sintering process, ceramic membranes are usually hydrophilic in nature due to surface hydroxyl groups (-OH); however, during sintering process at high temperature, the surface of the membrane changes to hydrophobic. Composite membranes were also prepared to obtain the hydrophilic modification of the membrane surface.[20]

Mittal *et al.*[20] prepared hydrophilic ceramic-cellulose acetate membrane and tested its separation ability with oil-water emulsions. The oil rejection of 92.54 % was achieved with the feed concentration of 200 mg/L in a dead-end flow filtration. In another work, $Al_2O_3$ supported $TiO_2$ membrane was developed using $Ti(SO_4)_2$ as a precursor by in-situ hydrolysis method and intended to treat oil-water emulsions.[21] The membrane showed around 99.75 % rejection for the oil concentration of 4000 mg/L in a cross flow filtration.[21] Zhou *et al.*[19] fabricated $ZrO_2$ membrane on tubular $Al_2O_3$ support using $ZrCl_4$ as a raw material via in-situ precipitation method to treat stable oil-in-water emulsions. The prepared membrane demonstrated 97.8-99.2% rejection for the oil concentration of 9-13 mg/L in a cross flow filtration. Yang *et al.*[7] investigated the separation of oil contaminated water with $ZrO_2$/α-$Al_2O_3$ membrane and 99.8% of oil rejection was obtained with the feed oil concentration of 5000 mg/L in a cross flow filtration. The literature review clearly revealed that hydrophilic membranes possess several advantageous to conduct filtration tests for the oil-water emulsions, which includes less fouling and better oil rejection. It is noteworthy to mention that most of the hydrophilic modified membranes prepared on α-$Al_2O_3$ support, which is expensive. In view of such research developments, the present work emphases on the utility of the modified and unmodified ceramic membranes fabricated using low cost raw materials for application of oily wastewater treatment.

The present work describes the microfiltration of oil-in-water emulsion with ceramic support, $TiO_2$ and γ-$Al_2O_3$ composite membranes. Ceramic support was manufactured by means of an uniaxial dry pressing technique with clay powders available locally. $TiO_2$ and γ-$Al_2O_3$ coating on ceramic support were carried out separately using $TiCl_4$ and $AlCl_3$ as a source material, respectively, by the hydrothermal treatment method. Prepared ceramic membranes were charactyerized to evaluate porosity, morphology, and permeability of pure water. The performance of the membranes was tested by separation of oil from synthetic oil-

in-water emulsion, in which the effect of feed concentration and applied pressure on the removal efficiency (%) and permeate flux was examined.

## 2. Materials and methods

### 2.1. Materials

The clay powders (feldspar, kaolin, pyrophyllite, ball clay and quartz,) were collected from Kanpur, India. Calcium carbonate, polyvinyl alcohol (PVA), aluminium chloride (99.5% pure, $AlCl_3.6H_2O$) and aqueous ammonia solution (25 wt. %) were supplied by Merck (I) Ltd., Mumbai, India. Titanium tetrachloride ($TiCl_4$, 99.5% pure) was purchased from Loba Chemie, Mumbai, India. Crude oil used in this work was procured from IOCL Refinery, Guwahati, India. The Millipore system (ELIX-3) was used for Millipore water collection.

### 2.2. Preparation of membranes

The manufacturing procedure for ceramic support was adopted from our earlier work.[18] Firstly, the required composition of clay powders was mixed with PVA solution in a ball mill. After that, 22 g of powder was taken in a steel die and dry compacted through uniaxial pressing at 50 MPa load using hydraulic press. Then the resulted circular shaped ceramic support was subjected to a sequence of drying in a hot air oven at 100 °C for the duration of 24 h, 200 °C for 24 h to remove complete moisture and lastly, support was sintered for 6 h at the temperature of 950 °C within the furnace. Then the top and bottom surfaces of the support were polished with the help of SiC (C-220) abrasive paper. This was done to get a smooth surface and support was sonicated with water in the sonication bath (Make: Elma (India), Model: T460) to take out free particles formed during the course of polishing.

For the preparation of $TiO_2$ membrane, $TiCl_4$ solution was prepared by dropwise addition of $TiCl_4$ to the Millipore water under constant stirring at room temperature. An aqueous ammonia solution was added dropwise to $TiCl_4$ solution until the resulting solution pH reached 9.0. The above prepared solution was transferred to Teflon coated stainless steel (SS) autoclave reactor containing the above prepared ceramic support and the reactor was kept in an oven to conduct hydrothermal treatment at 160 °C for the duration of 12 h. Subsequent to treatment, the reactor was kept for natural cooling in an open atmosphere until it reaches the temperature of 25 °C. The coated membrane and powder sample obtained from the reactor were washed and dried at 110 °C for 12 h. Finally, both the membrane and as-synthesized powder were calcined at 400 °C for the duration of 3 h at a heating rate of 1 °C/min. The obtained $TiO_2$ membrane and powder were used for characterization.

Similarly, $\gamma$-$Al_2O_3$ membrane was prepared by hydrothermal method using $AlCl_3$ as a starting material. 4 wt. % $AlCl_3$ solution was prepared and an aqueous ammonia solution was added dropwise into the $AlCl_3$ solution with continuous stirring until the pH of the solution reached 8.0. Then the solution was transferred to a Teflon coated SS autoclave reactor and support was also placed in the reactor. The hydrothermal reaction was performed at 150 °C for 8 h. The membrane and as-synthesized powder were calcined at 600 °C for 3 h.

**2.3. Characterization**

Thermal degradation behavior of as synthesized powders was analyzed in Netzsch thermo gravimetric analyzer (Make: Netzsch, Model: STA449F3A00) in argon atmosphere with the temperature increment of 10 °C/min. The X-ray diffraction (XRD) analysis was acquired at 2θ values of 10-80° using a scanning rate of 0.05 °C/s in an equipment (Make: Bruker, Model: D8 ADVANCE) with Cu K$\alpha$ (λ=0.154506 nm) radiation operating at 40 kV and 40 mA. The crystallite size was calculated from X-ray diffraction patterns using Debye-

Scherrer equation, $D = K\lambda/(\beta\cos\theta)$, where $\lambda$ is the wavelength of the X-ray radiation ($\lambda$ = 0.154506 nm), K is a constant (0.9), $\beta$ is the peak full width at half maximum height, and $\theta$ is the diffraction angle. The particle size distribution (PSD) of $TiO_2$ and $\gamma$-$Al_2O_3$ sols were measured using Delsa nano C (Beckman Coulter). FTIR spectra of the prepared $TiO_2$ and $\gamma$-$Al_2O_3$ powders were analyzed using Shimadzu Fourier Transform Infrared Spectrosopy (FTIR) (Model: IRAffinity-1) to identify the functional groups present in the prepared powders. Nitrogen adsorption/desorption isotherms for calcined $TiO_2$ and $\gamma$-$Al_2O_3$ powder samples were determined at -196 °C using the BET method in the instrument, Quantachrome surface area and pore size analyzer (Make: Quantachrome, Model: Autosorb-IQ MP). Before $N_2$ adsorption/desorption analysis, both the samples ($TiO_2$ and $\gamma$-$Al_2O_3$ powder) were completely degassed under the temperature of 200 °C with 3 h duration. The structural morphology of the support and membranes was visually analyzed using (FESEM) field emission scanning electron microscopy (Make: Zeiss, Model: Sigma) instrument. Contact angle measurements for ceramic support, $TiO_2$ and $\gamma$-$Al_2O_3$ membranes were conducted using Drop shape analyzer (Make: Kruss, Model: DSA25) by sessile drop method with 4 µL volume of water droplet at a falling rateof 0.16 mL/min and framerate at 16. Archimedes' principle was considered as a standard method to determine the porosity of the ceramic membrane using water as a wetting medium.[22]

In order to evaluate the pore size of ceramic support and membranes, the permeation of $N_2$ gas through these membranes and support was carried out using an in-house made permeation set up as shown in Fig. 1 (a). The setup consists of a tubular shaped hollow top dome ended with circular shape (stainless steel) and at bottom, a circular shaped flat plate has a facility to place the membrane inside the flat plate and it was airtight by means of rubber gaskets. Then the setup was pressurized at various applied pressures by using $N_2$ gas and the outlet gas flow rate was calculated by using digital gas flow meter (Make: Agilent

Technologies, Model: ADM 1000 Universal Gas Flowmeter), which was connected to the outlet of the bottom flat plate. Each test was carried out at 25°C and before every test; the whole setup was checked for air leakage by dipping the setup in the detergent solution contained bucket. After finding out no leakage in the set up, then $N_2$ gas permeation tests were carried out. From the nitrogen permeation experiments, the measured data corresponds to flow rate (Q) versus applied pressure (ΔP) that was generated for ceramic support and membranes. The nitrogen gas effective permeability factor (K) of ceramic support and membranes was derived from the gas permeation data and average pore radius ($r_g$) was calculated as follows[25] :

$$K = 2.133\frac{r_g v}{l_p q^2} + 1.6\frac{r_g^2}{l\eta q^2}P \qquad (1)$$

Where, P is the average pressure acting on the membrane, ν denotes the molecular mean velocity of the gas (m/s), η describes the viscosity of gas (Pa s), q denotes the tortuosity, lp represents the length of the pore (m) and K denotes the effective permeability factor.

The effective permeability factor is calculated using the following expression:

$$K = \frac{P_2 Q}{S\Delta P} \qquad (2)$$

Where, ΔP denotes the applied pressure, Q represents the volumetric flow rate ($m^3/s$), $P_2$ is the membrane pressure at permeate side and S denotes the permeable area of the membrane.

The average pore size of the membrane can be obtained from the following expression:

$$r_g = 1.333\frac{B}{C}v\eta \qquad (3)$$

Where B and C are the intercept and slope, respectively, obtained from the expression (1).

**2.4. Pure water permeation study**

The pure water permeability and its flux of the membrane were determined using homemade dead-end filtration setup as illustrated in Fig.1(b).[18,23,24] Before the test, Millipore water was passed all the way through the membrane pores by applying a maximum working pressure of 414 kPa to take out unbound particles that exist within the pores. After that, the flux of pure water was determined by applying pressures in the ranges of 69-345 kPa. At every working pressure, first 50 mL of water was disposed and time taken for the collection of next 50 mL of water was utilized to measure the pure water flux with the help of below relation:

$$J_w = \frac{Q}{A\Delta T} \qquad (4)$$

Where, A represents the overall area of membrane surface available for filtration, $J_w$ represents flux of water, $\Delta T$ indicates the permeate collection time and Q denotes the permeated water quantity.

All the tests were carried out minimum five times and the average value is reported. The hydraulic permeability of the membrane is obtained from water permeation data, which is regressed by linear curve. Experiments were performed for three different membranes prepared from the same composition for estimating the general membrane characteristics and performance.

**2.5. Microfiltration of oil-in-water emulsions**

The stable oil-in-water emulsions having the concentrations of 50-250 mg/L were produced using crude oil in a sonication bath (Make: Elma (India), Model: T460) with intended time duration of 15-25 h at 25 $^{o}$C. Generally, crude oil contains natural surfactant, which helps to make highly stable emulsion. The emulsion stability is confirmed on the basis of vanishing oily layer on top of the water surface. Then the droplet size distributions of prepared four different concentrations of oil-in-water emulsions (50-250 mg/L) were

measured with the instrument, particle size analyzer (Make: Malvern, UK; Model: Master Sizer 2000).

The prepared support and membranes were applied to remove oil from the oil-in-water emulsions using dead-end flow setup (see Fig.1(b)). Each experiment was conducted using 150 mL quantity of feed oil solution in the experimental setup. For every applied pressure, the first 10 mL of the collected permeate was rejected and the time taken for the collection of second 10 mL of permeate was used to measure the permeate flux. The below expression was used to estimate the oil rejection values of the membrane:

$$R(\%) = \frac{C_f - C_p}{C_f} \times 100 \qquad (5)$$

Where, $C_p$ denotes the concentration of oil in the permeate and $C_f$ denotes the concentration of oil in the feed. UV–vis spectrophotometer (Make: Thermo Scientific, United States; Model: Spectrascan, UV 2300) was used to measure the concentration of oil in permeate and feed at a wavelength of 236 nm.

The membranes were regenerated by following steps:

i. After performing microfiltration test at a pressure, then the membrane was washed using the detergent solution (surf excel) to take out the sticky oil on the membrane surface.

ii. After that, the membrane was kept for washing in Millipore water contained beaker for about 1 h at 25 °C.

iii. Finally, the pure water was flushed through the membrane at a maximum pressure until to gain its initial flux, and then the next microfiltration test was carried out with this cleaned membrane.

## 3. Results and discussion

### 3.1. Particle size distribution (PSD)

Fig. S1 (Supplementary data) demonstrates the particle size distribution of synthesized sols ($TiO_2$ and $Al_2O_3$). Generally, smaller size particles deposite uniformly on the support in more quantity and block the pores of the support and even some particles may penetrate through larger pores.[26] Sols with larger particle sizes may not form uniformly on the support and mostly create patches on the surface of the support.[27] It can be noticed from Fig. S1 (Supplementary data) that the particle sizes of $TiO_2$ and $Al_2O_3$ sol are in the range of 0.3382-0.4777 μm, and 7.192-16.912 μm, respectively, while the volume median diameter is found to be 0.016225 and 0.001698 μm for $TiO_2$ and γ-$Al_2O_3$, respectively. The preparation of the composite ceramic membrane would be satisfied using the particle sizes of the aforesaid range.

### 3.2. $N_2$ adsorption-desorption isotherm

Nitrogen adsorption-desorption isotherm and BJH pore size distributions of γ-$Al_2O_3$ and $TiO_2$ powder are shown in Fig. S2 (Supplementary data). According to the IUPAC classification, isotherm of mesoporous $TiO_2$ and γ-$Al_2O_3$ powder matches with a type IV group (with H2 hysteresis loop). It also displays that $TiO_2$ and γ-$Al_2O_3$ particles possess complex and interconnected pores of different sizes and shapes.[28] The pore size distributions of $TiO_2$ and γ-$Al_2O_3$ are measured based on the desorption isotherm data by using the technique of BJH as depicted in Fig. S2 (Supplementary data). From these plots, it is evident that the $TiO_2$ and γ-$Al_2O_3$ particles contain only mesopores. These also show an unimodel distribution with pore radius of 1.54-73.85 nm for γ-$Al_2O_3$ and 0.15-7.36 nm for $TiO_2$. Moreover, 90 % of pores are having the size less than 10 nm for γ-$Al_2O_3$ (1.5 nm for $TiO_2$).

BET surface area (SA) along with the pore volume (PV) of $TiO_2$ is evaluated as 105.7 $m^2/g$ (200.3 $m^2/g$ for γ-$Al_2O_3$) and 0.4037 ml/g (0.4495 ml/g for γ-$Al_2O_3$), respectively.

### 3.3. FTIR

FTIR spectra of $Al_2O_3$ and $TiO_2$ powders (before and after calcination) are shown in Fig. S3 (Supplementary data). For as-synthesized $Al_2O_3$ powder (before calcination), bands at 744, 628 and 1070 $cm^{-1}$ are allotted to boehmite, and similar kind of characteristic results are reported in literature.[30] Bending modes of Al-O-H is observed at 1070 $cm^{-1}$ for symmetric and 1160 $cm^{-1}$ for asymmetric.[31] The OH torsional mode is not identified at 750 $cm^{-1}$ due to the overlap of stretching vibrations of Al-O with OH. The intense band at 1402 $cm^{-1}$ and 1722 $cm^{-1}$ represents bending of physically presented water and the stretching mode of adsorbed water molecule can be seen at 3118 $cm^{-1}$.[32] The weak band observed at 2010 $cm^{-1}$ corresponds to a combination band in boehmite, which is not observed in the calcined sample (see Fig. S3, after calcination). In general, alumina can exhibit various kinds of coordination with an oxygen molecule from its oxides.

In the as-synthesized $Al_2O_3$ sample (before calcination), the bands of stretching modes for $AlO_6$ are observed at 744 and 628 $cm^{-1}$.[33] After calcination of $Al_2O_3$ sample at 600 °C, the bands at 1070 and 2010 $cm^{-1}$ are disappeared, which confirms the formation of γ-$Al_2O_3$ (see Fig. S3). For γ-$Al_2O_3$ (after calcination), the narrow bands identified at 1644, 1525, and 3618 $cm^{-1}$ are because of the adsorbed water present in the sample. The peaks observed at 592 and 867 $cm^{-1}$ correspond to $AlO_6$ and $AlO_4$, respectively. The above result corroborates that γ-$Al_2O_3$ ($Al_2O_3$ after calcination sample) has two kinds of Al-O structures i.e tetrahedral and octahedral, while $Al_2O_3$ powder before calcination is purely octahedral in nature.[34] In the case of $TiO_2$ samples, the band appeared around 460 $cm^{-1}$ corresponds to the Ti-O stretching.[35] For $TiO_2$ sample (before calcination), the bands noticed at 1402, 1630,

1752 $cm^{-1}$ are ascribed to stretching mode and the bands appeared at 3118 and 3436 $cm^{-1}$ represent bending modes of a physically adsorbed water molecule. The weak band observed at 2010 $cm^{-1}$ for $TiO_2$ sample (before calcination) is attributed to Ti-OH bond of the $Ti(OH)_4$ functional group, which disappears after calcination at 400 °C.

### 3.4. Thermo gravimetric analysis (TGA)

Fig. 2 illustrates the differential thermogravimetric (DTG) and thermogravimetric (TG) plots for $TiO_2$ and γ-$Al_2O_3$ powder samples. $TiO_2$ powder (before calcination) seems to undergo two different stages of weight loss during heating. The weight loss at <195 °C is due to the deliverance of physically adsorbed water present inside the pores of the powder. The second step of weight loss at temperature range of 195-350 °C is attributed to the structural change of the powder from $Ti(OH)_4$ to $TiO_2$. After 350 °C, the weight loss is negligible and hence, the calcination temperature for the fabrication of the membrane is fixed as 400 °C. In the DTG plot, an endothermic peak noticed around the temperature of 290 °C represents the loss of crystallization of the $TiO_2$ powder by changing its structure from titanium hydroxide to $TiO_2$. γ-$Al_2O_3$ sample (before calcination) undergoes step by step of weight loss in three stages during the heating process. The first stage of weight loss at less than 70 °C is due to the liberation of adsorbed water existing inside the powder and the second step of weight loss noticed between 70 °C and 250 °C corresponds to the evaporation of crystal water present in the powder, which is also clearly evidenced in the DTG curve around 125.5 °C. The third stage of weight loss observed from 250 °C to 550 °C is due to the dehydroxylation of the sample to γ-$Al_2O_3$. In the DTG graph, a peak (endothermic) at 334 °C corresponds to the decomposition of the sample to γ-$Al_2O_3$ powder.[29] The weight loss at >550 °C is negligible and therefore, the optimized calcination temperature is selected as 600 °C for the preparation of the γ-$Al_2O_3$ membrane.

### 3.5. XRD analysis

The XRD analysis was carried out to recognize whether any phase transformation occured during the course of sintering. The XRD patterns of powders ($TiO_2$, and γ -$Al_2O_3$) and the membrane support (before and after sintering) are presented in Fig. 3. During the sintering process, phase transformation usually occurs due to a series of reactions, and is also caused by the formation of new phases. Prior to sintering, there are few major phases seen in support, which are pyrophyllite, kaolin, calcium carbonate, feldspar, and quartz. Several phase changes take place within the support during the sintering process. However, the important phase conversion is the change of kaolinite to mullite through metakaolinite. It is ensured from the XRD patterns of sintered support, in which kaolin peaks are disappeared. The consistent peaks corresponding to quartz appear in both the support (before and after sintering). This clearly indicates that quartz is a thermally stable phase. Moreover, no significant weight loss is observed for quartz in TGA analysis.[1] During the sintering process, $CaCO_3$ is converted to CaO and $CO_2$, which is reflected in the XRD profile of after sintering sample. The new phase, wollastonite ($CaSiO_3$) is alse observed, that may be formed due to the reaction of amorphous silica with CaO.[36]

The XRD patterns of $Al_2O_3$ powder (before and after calcination) are illustrated in Fig. 3. XRD peaks of $Al_2O_3$ powder (before calcination) are good agreement with JCPDS PDF (File No. 21-1307), corresponding to the boehmite powder. The diffraction analysis of $Al_2O_3$ powder (after calcination) is observed as γ-$Al_2O_3$ phase, which is concurrence with the standard γ-$Al_2O_3$ phase of JCPDS PDF (File No. 10-0425). The presence of (311), (400) and (440) peaks in the calcined sample of $Al_2O_3$ confirm the existence of γ-$Al_2O_3$ nanocrystallites.[37] In order to determine the crystallite size of γ-$Al_2O_3$ powder samples (before and after calcination), three measurements were carried out for each sample synthesized in a single batch and the average value was reported with standard deviation. The

crystaline size of γ-$Al_2O_3$ (after calcination) from (400) peak is found to be 3.5±1.03 nm, while the crystalline size of before calcination sample is 2.3±0.92 nm, which is obtained from (020) peak. These values reveal the existence of nano γ-$Al_2O_3$ phase.[38] The XRD patterns of $TiO_2$ powder (before and after calcination) are also shown in Fig. 3. After calcination, XRD peaks of $TiO_2$ sample such as (101), (004), (020), (015), (024) match with JCPDS PDF File No. 21-1272 for anatase $TiO_2$. This reveals the formation of the nano-$TiO_2$ powder.[39]

### 3.6. Porosity

The procedure used for the measurement of porosity of membranes is well described in literature.[18,22] The below equation was used to calculate the porosity (ε) of the membrane:

$$\varepsilon = \frac{W_W - W_D}{W_W - W_A} \qquad (6)$$

Where, $W_A$ is the water saturated membrane weight measured in water (A refers to Archimedes), $W_W$ is the wet weight of the membrane (pores are filled with water under vacuum), $W_D$ is the dry weight of the membrane and ε is the porosity of the membrane. For every membrane, five experiments were conducted using the same composition membranes prepared at different batches and the average value was reported with standard error. The porosity of the support, $TiO_2$ and γ-$Al_2O_3$ membranes is found to be 45.57±0.65, 43.32±0.35 and 42.29±0.62%, respectively. These results elucidate that there is no significant difference in the porosity of the membranes. However, there is a variation between support and membranes, which is due to the formation of $TiO_2$ and γ-$Al_2O_3$ layers on support.

### 3.7. FESEM images of the membrane

FESEM images of support and membranes were depicted in Fig. 4 (a-c). It is clearly visible that the surface of support is coated with $TiO_2$ and γ-$Al_2O_3$ particles. The rough morphology resembles that there are no cracks and pin holes on the surface. In the images,

$TiO_2$ nanoparticles deposited on the ceramic support are shown in a circle symbol with an arrow mark and γ-$Al_2O_3$ layers are shown in a rectangular symbol with an arrow mark. Images with different magnifications display uniform $TiO_2$ and γ-$Al_2O_3$ coating on support. These layers change the surface character of the support from hydrophobic to hydrophilic nature. Therefore, it is useful to separate oil from oily wastewater. The hydrophilic membrane surface contributes to repel oil droplets from adhering to the membrane surface, and hence it reduces the membrane fouling. The pore size distribution of support and membranes was estimated from FESEM images using ImageJ software (http:// rsbweb.nih.gov/ij/download.html) and the obtained results are presented in the Fig. 5. The following equation was employed for the determination of the average pore size of the membrane ($D_{avg}$):[45]

$$D_{avg} = \frac{\sum_{i=1}^{n} n_i d_i}{\sum_{i=1}^{n} n_i} \qquad (7)$$

Where, $d_i$ represents the $i^{th}$ pore diameter (μm), n denotes the number of pores and $D_{avg}$ describes the average values of the membrane pore diameter (μm). It is apparent from Fig. 5 that the support and membranes have different porous structure with pore sizes ranging between 0.001 and 2.75 μm. From these pore size distributions, the average pore diameter of the support, $TiO_2$ and γ-$Al_2O_3$ membranes is estimated to be 1.01±0.036, 0.98±0.021 and 0.97±0.017 μm, respectively.

Pore size of the ceramic support and composite membranes was also determined by $N_2$ gas permeation study. Fig. 6 depicts the effective permeability factor versus average pressure for ceramic support and composite membranes. The smallest pore size and the lowest value of effective permeability factor are noticed for the $TiO_2$ membrane. The average pore size obtained from $N_2$ gas permeation is 0.981±0.014, 0.877±0.029 and 0.786±0.041 μm

for ceramic support, $TiO_2$ and $\gamma$-$Al_2O_3$ membrane, respectively, whereas the mean pore size of ceramic support, $TiO_2$ and $\gamma$-$Al_2O_3$ membrane determined from FESEM analysis is 1.01±0.036, 0.98±0.021 and 0.97±0.017 μm, respectively. The difference might be due to the fact that the FESEM analysis deals only with the surface pores of the membrane, while gas permeation study provides the size of inner pore channels (minimum passage, which is the neck of a funnel like shape, to pass through the gas) of the membrane. The reducuction in pore sizes with the coating of $TiO_2$ and $\gamma$-$Al_2O_3$ particles on ceramic support is observed from both $N_2$ gas permeation and FESEM image analysis.

Fig. 4 (d-f) shows the contact angle of the ceramic support, $TiO_2$ and $\gamma$-$Al_2O_3$ membrane. Five measurements were carried out for each membrane at different locations and the average value was reported with standard error. The contact angle measurement was done to know the wettability and surface interaction of the membrane surface with liquid. The contact angle indicates the degree of wetting when a solid and liquid interact. A small contact angle ($<< 90°$) corresponds to high wettability, while a larger contact angle value ($>> 90°$) corresponds to low wettability. Generally, for super hydrophilic surfaces, the water contact angle (WCA) is less than 0° and at this condition, the solid surface exhibits the droplet shape into a flat puddle due to complete wetting of the surface. It is well documented in literature that for super hydrophobic surfaces, water contact angles are usually greater than 150°, and it will show almost no contact between the water droplet and the solid surface.[40-44] The contact angle of the ceramic support, $TiO_2$ and $\gamma$-$Al_2O_3$ membrane is found to be 77.07±2.37°, 14.57±0.54° and 19.43±1.13°, respectively. The obtained results clearly point out that the prepared $TiO_2$ membrane is more hydrophilic in nature. Fig. 4 (d-f) shows that a small contact angle is observed when the water spreads on the $TiO_2$ membrane, while a larger contact angle is observed when the water spreads on the ceramic support.

Moreover, the contact angle of $TiO_2$ membrane is 14.57±0.54°, indicating that the wetting of the surface is favorable, and the fluid will spread over a large area on the surface of the $TiO_2$ membrane. In contrary, the contact angle of ceramic support is 77.07±2.37°, signifying that the wetting of the surface of ceramic support is unfavorable. Therefore, the fluid will minimize its contact with the support surface and form a compact liquid droplet. The contact angle of ceramic support is more than that of the prepared membranes; hence the support has less hydrophilic in nature compared to $TiO_2$ and γ-$Al_2O_3$ membranes. The hydrophilicity of the prepared membranes varies in the following trend: $TiO_2$ > γ-$Al_2O_3$ > Ceramic support.

### 3.8. Water flux and hydraulic permeability

The water flux or hydraulic permeability of the membrane will depend on three factors, such as hydrophilic nature of the membrane surface, pore size and porosity.[46] Fig. 7 shows the effect of applied pressure on the water flux. Despite the fact that, the pure water flux of the support and membrane increases proportionately with an increment in the applied pressure, which is consistent with the results obtained by Shokrkar *et al.*[47] The flux of $TiO_2$ coated membrane is higher than that of ceramic support. This is mostly because of changes in the hydrophilic character of the surface of support by $TiO_2$ coating. A similar result was also reported in the literature.[4,19,48] $TiO_2$ nanoparticles coating did not decrease the water flux, but increased the hydrophilic character of the support surface. The water flux of the $TiO_2$ membrane is more than that of the γ-$Al_2O_3$ membrane because the hydrophilic nature of the $TiO_2$ coating is more than that of γ-$Al_2O_3$ coating and also the pore size reduction is slightly higher in case of γ-$Al_2O_3$ membrane. The hydraulic permeability value is estimated to be $2.59\times10^{-9}$, $3.12\times10^{-9}$, and $3.003\times10^{-9}$ ($m^3/m^2$ s Pa) for γ-$Al_2O_3$ membrane, $TiO_2$ membrane and support, respectively. It is worth to mention that the average pore diameter of the support, $TiO_2$ and γ-$Al_2O_3$ membrane is 0.981±0.014, 0.877±0.029 and 0.786±0.041 μm, respectively,

which is determined from $N_2$ gas permeation experiments. The variation in water permeability of the membranes is due to hydrophilic modification of the surface of ceramic support.

### 3.9. Separation of oil-in-water emulsion

Fig. 8 demonstrates the droplet size distribution of oil-water emulsion at different feed concentrations. For all the concentrations, it can be noticed that the droplet size of emulsion varies in the range of 0.05-100 μm. The average droplet size (in diameter) of emulsion is determined as 0.771, 0.989, 6.037 and 6.928 μm of 50, 150, 200 and 250 mg/L of oil concentration, respectively.

#### *3.9.1. Effect of applied pressure on oil separation*

The performance of the membrane was tested by altering the applied pressures from 69 to 345 kPa for a fixed concentration of 200 mg/L. Fig. 9 reveals that the rejection decreases with increasing applied pressure for all the membranes. The reason for this trend is that higher pressures facilitate the enhancement of wetting and coalescence of oil droplets by increasing forced convection. This possibly allows a few oil droplets to elapse all the way through the pores of the membrane to arrive at permeate stream side resulting decreased rejection. This kind of results is well documented in the literature.[18,49,50] All the membranes display around 96-99% rejection and the maximum rejection is obtained with $TiO_2$ membrane when compared to the $\gamma$-$Al_2O_3$ membrane and support.

The hydrophilic membranes show more selectivity towards water due to which the permeability of the $TiO_2$ and $\gamma$-$Al_2O_3$ membrane is found to be higher when compared to the hydrophobic support.[51] This reveals that the hydrophilic character and nanoparticles coating on the support are responsible for both permeate flux and oil removal (%) in the treatment of

oil-in-water emulsion. Among all the studied membranes, $TiO_2$ membrane is better with respect to permeate flux and rejection.

### *3.9.2. Effect of feed concentration on oil separation*

The potential of the $TiO_2$ and $\gamma$-$Al_2O_3$ membranes was investigated by treating synthetic oil-in-water emulsions with oil concentrations of 50, 150, 200 and 250 mg/L at an applied pressure of 207 kPa. Fig. 10 depicts the effect of oil concentration on permeate flux and rejection of the $TiO_2$ and $\gamma$-$Al_2O_3$ membranes. In general, the oil droplet size and density increase with increasing feed concentration. This is a reason for the increased rejection at higher concentration. The droplet size of the emulsion varies between 0.05 to 100 μm for all the studied concentrations (50-250 mg/L). Then the resulted average droplet size of oil (in diameter) is determined as 0.771, 0.989, 6.037 and 6.928 μm for oil concentration of 50, 150, 200 and 250 mg/L, respectively. It is clear from Fig. 5 that the support and membranes have different porous structure with pore sizes ranging between 0.001 and 2.75 μm. From this pore size distributions (Fig. 5), the average pore diameter of the support, $TiO_2$ and $\gamma$-$Al_2O_3$ membranes is estimated to be 1.01±0.036, 0.98±0.021 and 0.97±0.017 μm, respectively. The average pore size obtained from $N_2$ gas permeation is 0.981±0.014, 0.877±0.029 and 0.786±0.041 μm for ceramic support, $TiO_2$ and $\gamma$-$Al_2O_3$ membrane, respectively. The volume median diameter of the oil droplet (0.771-6.928 μm) is higher than the pore diameter of the support (0.981±0.014 μm) and membranes (0.877±0.029, 0.786±0.041 μm), suggesting a greater possibility for the rejection of oil droplets. The oil droplet sizes greater than the pore sizes of the membrane are retained on the membrane surface during microfiltration of oil-water emulsion according to sieving mechanism. In general, the permeability depends on the pore diameter as well as surface characteristics of the membrane pores. If the membrane possesses a superior percentage of pore sizes that are larger than the emulsion droplet sizes along with greater hydrophilic surface, then the membrane will display better removal

efficiency with good permeate flux, which is highly essential for an industrial point of view. A higher concentration of oil leads to coalescence of oil droplets forming a bigger droplet that result in higher rejection. When oil concentration increases from 50 to 250 mg/L, the permeate flux decreases because the size of oil droplet is higher than the pore diameter of the membranes at higher concentrations. Also, this may be due to the pore blocking mechanism of oil with the membrane.[20, 23] For hydrophilic membranes, the bond between oil droplets and membrane surface is weak and can be broken easily because of the hydrophilic nature of the membrane surface. Therefore, oil rejection and flux of $TiO_2$ and $\gamma$-$Al_2O_3$ membranes are higher than that of the support having a hydrophobic surface.[52]

The performance of the $TiO_2$ membrane (98.95% of oil rejection as well as $8.481\times10^{-5}$ $m^3/m^2$ s of permeate flux for the feed oil concentration of 200 mg/L at 69 kPa) and $\gamma$-$Al_2O_3$ membrane (oil rejection of 98.46 % with permeate flux of $6.1185\times10^{-5}$ $m^3/m^2$ s for the feed oil concentration of 200 mg/L at an applied pressure of 69 kPa) is comparable with the available literature data.[23] A clay based ceramic membrane developed by Vasanth *et al.*[23] showed about 96% rejection with permeate flux of $0.006\times10^{-5}$ $m^3/m^2$ s for the feed oil concentration of 200 mg/L at an applied pressure of 69 kPa. A maximum oil removal of 92.54% was obtained using cellulose acetate membrane having average pore size of 0.028 µm at an applied pressure of 138 kPa for the oil-in-water emulsion concentration of 200 mg/L. [20] In the work reported by Singh et al.[53], the polyamide membrane with the mean pore size of 1.116 µm displayed ~ 97.80% removal efficiency of oil with permeate flux of $0.0335\times10^{-4}$ $m^3/m^2$ s. Salahi et al.[50] investigated the ability of the polysulfone membrane (with an average pore diameter of 0.1 µm) to remove oil from oil-in-water emulsion (200 mg/L) and the membrane demonstrated about 95% oil rejection. Till date, only few researchers have investigated upon the performance of ceramic membrane technology for the separation of oil from its emulsions. A key analysis of the available literature offers several

information. Firstly, literature is highly focused towards higher concentration of oil-in-water emulsions treatment applications, but not lower concentration, which are also important from the perspective of industrial waste disposal. Therefore, low cost ceramic membrane technology might be promising in such situations. Cui et al.[8] studied upon the efficacy of α-$Al_2O_3$ membrane with the mean pore size of 1.2 μm for oil-in-water emulsion applications. They presented a detailed investigation with respect to oil removal from oil-in-water emulsions (100 mg/L) at an applied pressure of 100 kPa. Then they achieved 98.80% of oil rejection with $0.1667\times10^{-4}$ $m^3/m^2$ s of permeate flux. The research work of Song et al.[56] has proven that coal membrane with the mean pore size of 1 μm was also efficient for the treatment of 120 mg/L feed oil at an applied pressure of 100 kPa. The permeate flux of $0.1786\times10^{-4}$ $m^3/m^2$ s and oil removal of 97.80% were oberved. The polysulfone membrane (average pore size of 0.00362 μm) displayed oil separation efficiency of 97.57% and permeate flux of $0.2399\times10^{-4}$ $m^3/m^2$ s for the feed oil concentration of 100 mg/L and applied pressure of 69 kPa.[57]

A vital concern of the fabricated ceramic membranes is to achieve 100% separation efficiency with good flux, which is very much dependent on pore size distributions, morphologies, suface characteristics (hydrophilic/hydrophobic) and feed concentration of the oil-in-water emulsions. Thus, it is apparent that a significant amount of research activity needs to be dovetailed towards the development and application of ceramic membranes for oil-in-water emulsion filtration applications. In view of this, a systematic investigation that accounts for the modification of surface characteristics of the membrane to suite the desired application is very important.

The resistances of different membranes to survive in severe ecological surroundings and possessing extensive serviceable life are of important task. In this context, clay based membrane is a unique choice that can be used for many industrial applications, since it was

tested and justified to have a superior serviceable life and endurance for the treatment of wastewater. However, for comparable view point, it can be noticed that the highest oil removal ability of fly ash membrane recorded by Fang et al.[59] was 95.30% with permeate flux of $0.4417\times10^{-4}$ $m^3/m^2$ s, which is very low. Therefore, this effort involved to concentrate on productive and economical manufacturing methods as well as coating materials to attain an excellent quality of membrane, which can provide better separation efficiency and superior permeate flux than the published data are highly valuable.

It can be concluded that the studied membranes demonstrate better performance on the basis of rejection and flux as compared to other membranes listed in literature. Table 1 summarizes the comparison of present membrane performance for the separation of oil from the oil-in-water emulsions with the data available for different membranes listed in literature.[8,18,42,45-52] It can be observed that the rejection values of the membranes are comparable with those membranes reported in literature. In comparison with support, $TiO_2$, $Al_2O_3$ membranes display the highest oil removal efficiency along with good flux owing to the enhanced hydrophilic characteristics of the surface modified support. Amongst the available data, the result obtained for the $TiO_2$ membrane is the finest in terms of superior permeate flux ($0.8481\times10^{-4}$ $m^3/m^2$ s) and maximum oil rejection (98.96%) for the feed oil concentration of 200 mg/L at an applied pressure of 69 kPa. The membrane performance ability is estimated on the basis of it's permeate flux and rejection values, which are found to be acceptable range and hence, the fabricated composite membranes are opined to be chosen for more efficient in separation of oil from oil-in-water emulsions.

## 4. Conclusions

Clay based ceramic support has been successfully fabricated by uniaxial pressing method and sintered at 950 $^oC$. $TiO_2$ and $\gamma$-$Al_2O_3$ composite membranes were fabricated

using inexpensive titanium tetrachloride and aluminium chloride, respectively. Hydrothermal method was adopted to coat the $TiO_2$ and $\gamma$-$Al_2O_3$ nanoparticles on the ceramic support and modified the surface character of the support from hydrophobic to hydrophilic. The porosity of support, $TiO_2$ and $\gamma$-$Al_2O_3$ membranes was found to be 45.57±0.65, 43.32±0.35 and 42.29±0.62%, respectively. The average pore diameter of the support, $TiO_2$ and $\gamma$-$Al_2O_3$ membranes was estimated to be 0.981±0.014, 0.877±0.029, 0.786±0.041 μm, respectively. The above prepared $TiO_2$ and $\gamma$-$Al_2O_3$ membranes showed better rejection and permeate flux in separation of oil-in-water emulsions than that of the ceramic support.

## Acknowledgment

We would like to express our sincere gratitude to the Central Instruments Facility of IIT Guwahati for helping us to perform FESEM analysis. Contact angle instrument used in this work was financially supported by a grant for Center of Excellence for Sustainable Polymers at IIT Guwahati from Department of Chemicals & Petrochemicals, Ministry of Chemicals and Fertilizers, Government of India.

## References

1 A. Ezzati, E. Gorouhi and T. Mohammadi, *Desalination,* 2005, **185,** 371-382.

2 T. Mohammadi, A. Pak, M. Karbassian and M. Golshan, *Desalination,* 2004 **168,** 201-205.

3 I. W. Cumming, R. G. Holdich and I. D. Smith, *J. Membr. Sci.,* 2000, **169,** 147-155.

4 F. L. Hua, Y. F. Tsang, Y. J. Wang, S. Y. Chan, H. Chuand and H. N. Sin, *Chem. Eng. J.,* 2007, **128,** 169-175.

5 S. R. H. Abadi, M. Sebzari, M. Hemati, F. Rekabdar and T. Mohammadi, *Desalination,* 2011, **265,** 222-228.

6 J. Zhong, X. Sun and C. Wang, *Sep. Purif. Technol.,* 2003, **32,** 93-98.

7 C. Yang, G. Zhang, N. Xu and J. Shi, *J. Membr. Sci.,* 1998, **142,** 235-243.

8 J. Cui, X. Zhang, H. Liu, S. Liu and K. L. Yeung, *J. Membr. Sci.,* 2008, **325,** 420-426.

9 A. Alem, H. Sarpoolaky, and M. Keshmiri*, J. Eur. Ceram. Soc.,* 2009, **29,** 629-635.

10 C. Falamaki, M. S. Afarani and A. Aghaie, *J. Eur. Ceram. Soc.,* 2004, **24,** 2285-2292.

11 K. A. DeFriend, M. R. Wiesner and A. R. Barron, *J. Membr. Sci.,* 2003, **224,** 11-28.

12 J. M. Benito, A. Conesa, F. Rubio and M. A. Rodriguez, *J. Eur. Ceram. Soc.,* 2005, **25,** 1895-1903.

13 Y. Yoshino, T. Suzuki, B. N. Nair, H. Taguchi and N. Itoh, *J. Membr. Sci.,* 2005, **267,** 8-17.

14 P. Wang, N. Xu and J. Shi, *J. Membr. Sci.,* 2000, **173,** 159-166.

15 Y. H. Wang, T. F. Tian, X. Q. Liu and G. Y. Meng, *J. Membr. Sci.,* 2006, **280,** 261-269.

16 Y. H. Wang, X. Q. Liu and G. Y. Meng, *Mater. Sci. Eng. A,* 2007, **445-446,** 611-619.

17 T. Tsuru, *Sep. Purif. Meth.,* 2001, **30,** 191-220.

18 P. Monash and G. Pugazhenthi, *Desalination,* 2011, **279,** 104-114.

19 J. Zhou, Q. Chang, Y. Wang, J. Wang and G. Meng, *Sep. Purif. Technol.,* 2010, **75,** 243-248.

20 P. Mittal, S. Jana and K. Mohanty, *Desalination,* 2011, **282,** 54-62.

21 Q. Chang, J. Zhou, Y. Wang, J. Liang, X. Zhang, S. Cerneaux, X. Wang, Z. Zhu and Y. Dong, *J. Membr. Sci.,* 2014, **456,** 128-133.

22 D. Laux, J. Y. Ferrandis, J. Bentama and M. Rguiti, *Appl. Clay Sci.,* 2005, **32,** 82-86.

23 D. Vasanth, G. Pugazhenthi and R. Uppaluri, *Sep. Sci. Technol.,* 2013, **48,** 849-858.

24 D. Vasanth, R. Uppaluri and G. Pugazhenthi, *J. Membr. Sci.,* 2011, **379,** 154-163.

25 J. Marchese and C. L. Pagliero, *Sep. Purif. Technol.*, 1991, **5**, 215-221.

26 T. H. V. Steenkiste, J. R. Smith and R. E. Teets, *Surf. Coat. Technol.,* 2002, **154,** 237-252.

27 K. Saleh and P. Guigon, *Coating and encapsulation processes in powder technology*, 1st edition, Elsevier, Handbook of powder technology, 2007, **11,** Chapter 7, 323-375.

28 Y. H. Wang, Y. Zhang, X. Q. Liu and G. Y. Meng, *J. Sol-Gel Sci. Technol.,* 2007, **41,** 267-275.

29 C. D. Jones and A. R. Barron, *Mater. Chem. Phys.,* 2007, **104,** 460-471.

30 A. Majhi, P. Monash and G. Pugazhenthi, *J. Membr. Sci.,* 2009, **340,** 181-191.

31 R. L. Frost, J. Kloprogge, S. C. Russell and J. L. Szetu, *Thermochim. Acta,* 1999, **329,** 47-56.

32 P.H. Colomban, *J. Mater. Sci. Lett.,* 1988, **7,** 1324-1326.

33 P. McMillan and B. Piriou, J. Non-Cryst. Solids, 1982, **53,** 279-298.

34 A. D. Cross, *An Introduction to practical IR Spectroscopy,* 2nd edition, Butterworth, London, 1964.

35 S. Li, Q. Shen, J. Zong and H. Yang, *J. Alloys Comp.,* 2010, **508,** 99-105.

36 A. Gualtieri, M. Bellotto, G. Artioli and S. M. Clark, *Phys. Chem. Miner.,* 1995, **22,** 215-222.

37 Y. Liu, D. Ma, X. Han, X. Bao, W. Frandsen, D. Wang and D. Su, *Mater. Lett.*, 2008, **62,** 1297-1301.

38 P. Padmaja, P. Krishnapillai and K. G. K. Warrier, *J. Porous Mater.,* 2004, 11, 147-155.

39 C. Wang, Y. Ao, P. Hou and J. Qian, *Colloids Surf. A: Physicochem. Eng. Asp.,* 2010, **360,** 184-189.

40 B. Arkles, *Hydrophobicity, Hydrophilicity and Silanes*, Paint & Coatings Industry magazine, Gelest Inc., Morrisville, PA, USA, 2006.

41 Y. Yuan and T.R. Lee, Contact angle and wetting properties In:G. Bracco and B. Holst (eds), *Surface Science Techniques*, Springer, Berlin, Heidelberg, 2013, Chapter 1, pp 3-34.

42 A.W. Adamson and A.P. Gast, Physical Chemistry of Surfaces, John Wiley & Sons, Inc., New York, USA, 1976.

43 L. Feng, S. Li, Y. Li, H. Li, L. Zhang, J. Zhai, Y. song, B. Liu, L. Jiang and d. Zhu, *Adv. Mater.*, 2002, **4**, 1857-1860.

44 J. Chinnam, D. Das, R. Vajjha and J. Satti, *Int Commun Heat Mass*, 2015, **62**, 1-12.

45 K. Suresh and G. Pugazhenthi, *Desalination Water Treat.,* 2014, DOI:10.1080/19443994.2014.979445.

46 N. A. Ochoa, M. Masuelli and J. Marchese, *J. Membr. Sci.,* 2003, **226,** 203-211.

47 H. Shokrkar, A. Salahi, N. Kasiri, and T. Mohammadi, *Chem. Eng. Res. Des.,* 2012, **90,** 846-853.

48 L. Yan, Y. S. Li, C. B. Xiang and S. Xianda, *J. Memb. Sci.,* 2006, **276,** 162-167.

49 P. Srijaroonrat, E. Julien and Y. Aurelle, *J. Membr. Sci.,* 1999, **159,**11-20.

50 A. Salahi, A. Gheshlaghi, T. Mohammadi and S. S. Madaeni, *Desalination,* 2010, **262,** 235-242.

51 D. V. Olegovich, S. I. Gilmanovich, B. S. Bonev, A. I. Shaukatovich and V. A. Nenov, *Energy Environ. Eng.,* 2013, **1,** 105-110.

52 M. Abbasi, A. Salahi, M. Mirfendereski, T. Mohammadi and A. Park, *Desalination,* 2010, **252,** 113-119.

53 V. Singh, M.K. Purkait and C. Das, *Sep. Sci. Technol.,* 2011, **46,** 1213-1223.

54 B. K. Nandi, R. Uppaluri and M. K. Purkait, *Sep. Sci. Technol.,* 2009, **44,** 2840-2869.

55 D. Vasanth, R. Uppaluri and G. Pugazhenthi, *J. Membr. Sci.,* 2011, **379,** 154-163.

56 C. W. Song, T. H. Wang, Y.Q. Pan, and J. S. Qiu, *Sep. Purif. Technol.,* 2006, **51,** 80-84.

57 B. Chakrabarty, A.K. Ghoshal and M.K. Purkait, *J. Membr. Sci.,* 2008, **325,** 427-437.

58 D. Vasanth, R. Uppaluri, G. Pugazhenthi, *Desalination,* 2013, **320,** 86-95.

59 J. Fang, G. Qin, W. Wei, X. Zhao and L. Jiang, *Desalination,* 2013, **311,** 113-126.

**Table 1:** Comparison of membrane performance with other reported membranes

| Membrane materials | Average pore size (µm) | Applied pressure (kPa) | Feed oil concentration (mg/L) | Permeate flux×$10^4$ ($m^3/m^2$ s) | Oil rejection (%) | Author |
|---|---|---|---|---|---|---|
| Clay materials | 1.21 | 69 | 200 | 0.0006 | 96.00 | Vasanth *et al.* (2013)[23] |
| Cellulose Acetate | 0.028 | 138 | 200 | 0.389 | 92.54 | Mittal *et al.* (2011)[20] |
| Clay materials | 0.98 | 345.4 | 200 | 0.7978 | 96.00 | Monash *et al.* (2011)[18] |
| Polyamide | 1.16 | 207 | 192 | 0.0335 | 97.80 | Singh *et al.* (2011)[53] |
| Clay materials | 0.285 | 69 | 125 | 0.054 | 98.40 | Nandi *et al.* (2009)[54] |
| Clay materials | 1.3 | 276.4 | 125 | 6.1084 | 85.00 | Vasanth *et al.* (2011)[55] |
| Coal | 1 | 100 | 120 | 0.1786 | 97.80 | Song *et al.* (2006)[56] |
| NaA1/α-$Al_2O_3$ | 1.2 | 100 | 100 | 0.1667 | 98.80 | Cui *et al.* (2008)[8] |
| Polysulfone | 0.00362 | 69 | 100 | 0.2399 | 97.57 | Chakrabarthy *et al.* (2008)[57] |
| Clay materials | 1.06 | 207 | 100 | 0.554 | 87.00 | Vasanth *et al.* (2013)[58] |
| Polysulfone | 0.1 | 300 | 78 | 0.2111 | 95.00 | Salahi *et al.* (2010)[23] |
| Fly ash | 0.77 | 100 | 75 | 0.4417 | 95.30 | Fang *et al.* (2013)[59] |
| α-$Al_2O_3$ | 0.2 | 125 | 26 | 0.6944 | 84.61 | Abadi *et al.* (2011)[5] |
| $TiO_2$ | 0.98 | 69 | 200 | 0.8481 | 98.96 | Present work |
| γ-$Al_2O_3$ | 0.97 | 69 | 200 | 0.6119 | 98.46 | Present work |

**List of Figures**

**Fig. 1** Schematic of **(a)** $N_2$ gas permeation test setup (1-$N_2$ gas cylinder, 2-pressure regulator, 3-connecting tube,4-pressure gauge, 5-membrane, 6-rubber gasket, 7-top compartment, 8-bottom base plate, 9-flow control valve and 10-digital flow meter) and **(b)** pure water permeation study set up (1-8 represent same as in **(a)**, 9-feed inlet and 10-permeate measuring cylinder).

**Fig. 2** TGA and DTG curves of as synthesized $TiO_2$ (A, a), and γ-$Al_2O_3$ (B, b) powder.

**Fig. 3** XRD profiles of the ceramic support, $TiO_2$, and $Al_2O_3$ powders before and after calcination (P-Pyrophyllite, M-Mullite, C-Calcium carbonate, F-Feldspar, CaO-Calcium oxide, W-Wollastonite, K-Kaolin and A-Anatase).

**Fig. 4** FESEM images (a,b,c) and contact angle (d,e,f) of support, $TiO_2$ and γ-$Al_2O_3$ membrane. (◯ -$TiO_2$ layer; □-γ-$Al_2O_3$ layer)

**Fig. 5** Pore size distribution of the support and membranes.

**Fig. 6** Effect of pressure on $N_2$ gas permeability of membranes and support.

**Fig. 7** Effect of pressure on pure water flux of membranes and support.

**Fig. 8** Droplet size distribution of oil-in-water emulsion.

**Fig. 9** Variation of permeate flux and rejection of oil with applied pressure for support (■, □), $TiO_2$ membrane (●, ○) and γ-$Al_2O_3$ membrane (▲, Δ).

**Fig. 10** Variation of permeate flux and rejection (%) of oil with feed concentration for support (■, □), $TiO_2$ membrane (●, ○) and γ-$Al_2O_3$ membrane (▲, Δ).

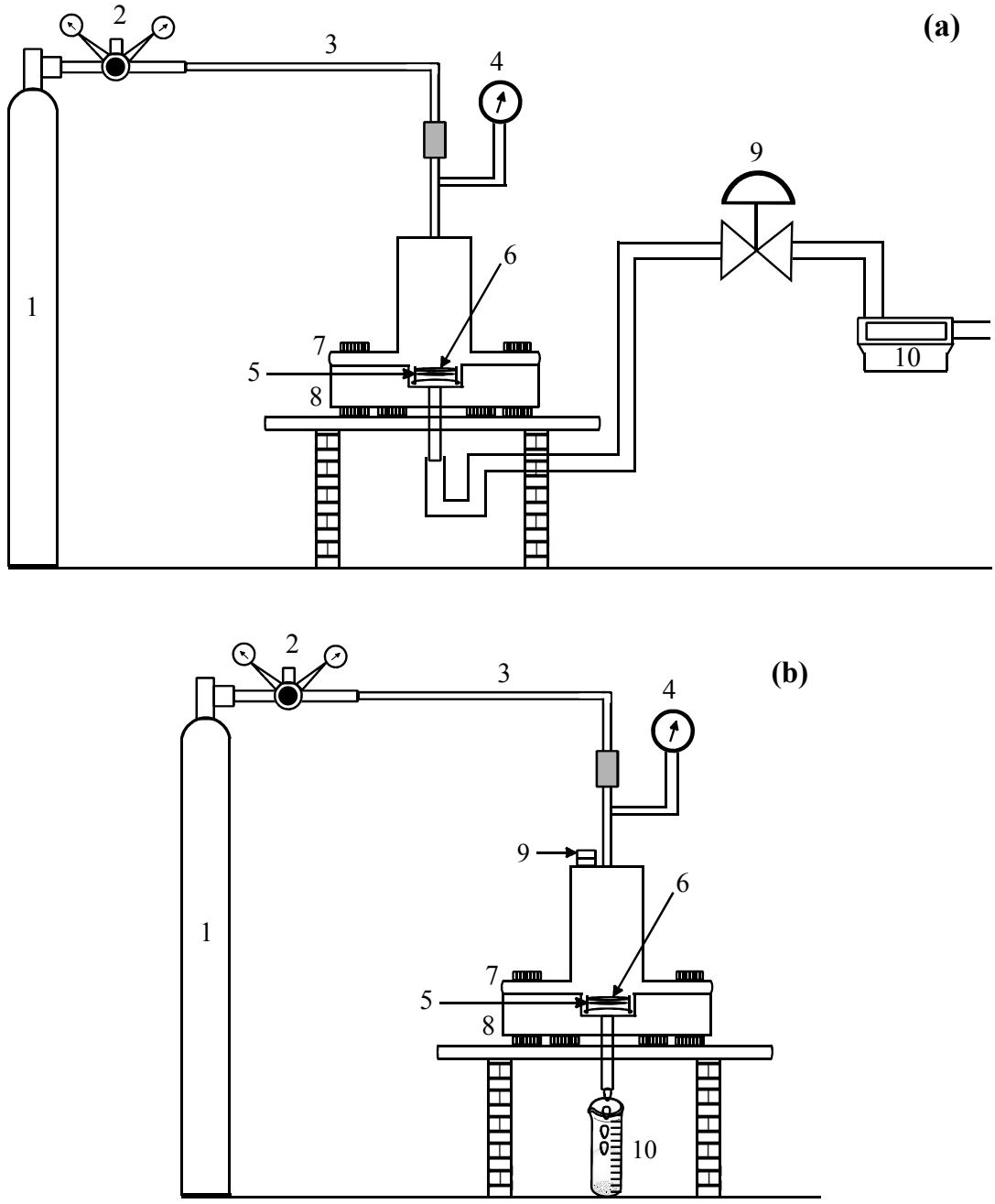


**Fig. 1** Schematic of **(a)** $N_2$ gas permeation test setup (1-$N_2$ gas cylinder, 2-pressure regulator, 3-connecting tube,4-pressure gauge, 5-membrane, 6-rubber gasket, 7-top compartment, 8-bottom base plate, 9-flow control valve and 10-digital flow meter) and **(b)** pure water permeation study set up (1-8 represent same as in **(a)**, 9-feed inlet and 10-permeate measuring cylinder).

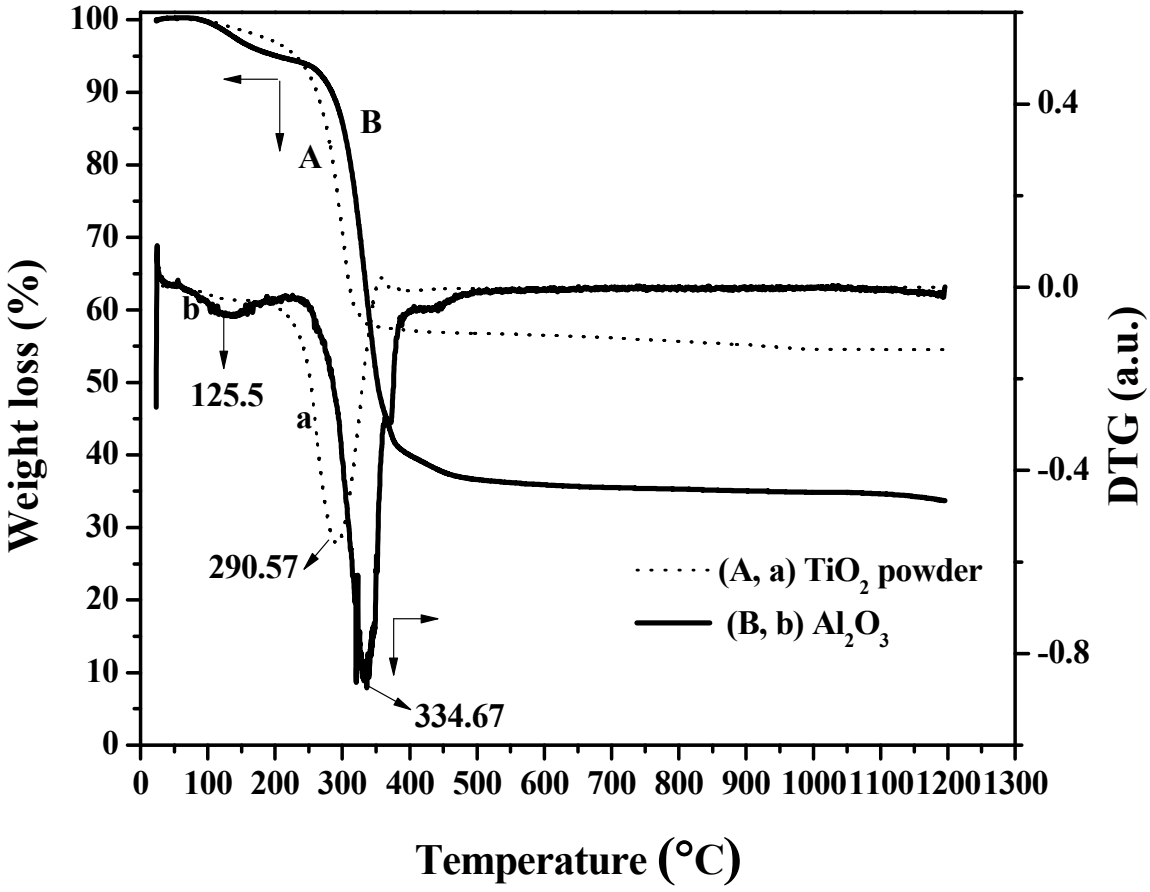


**Fig. 2** TGA and DTG curves of as synthesized (before calcination) $TiO_2$ (A, a), and $Al_2O_3$ (B, b) powder

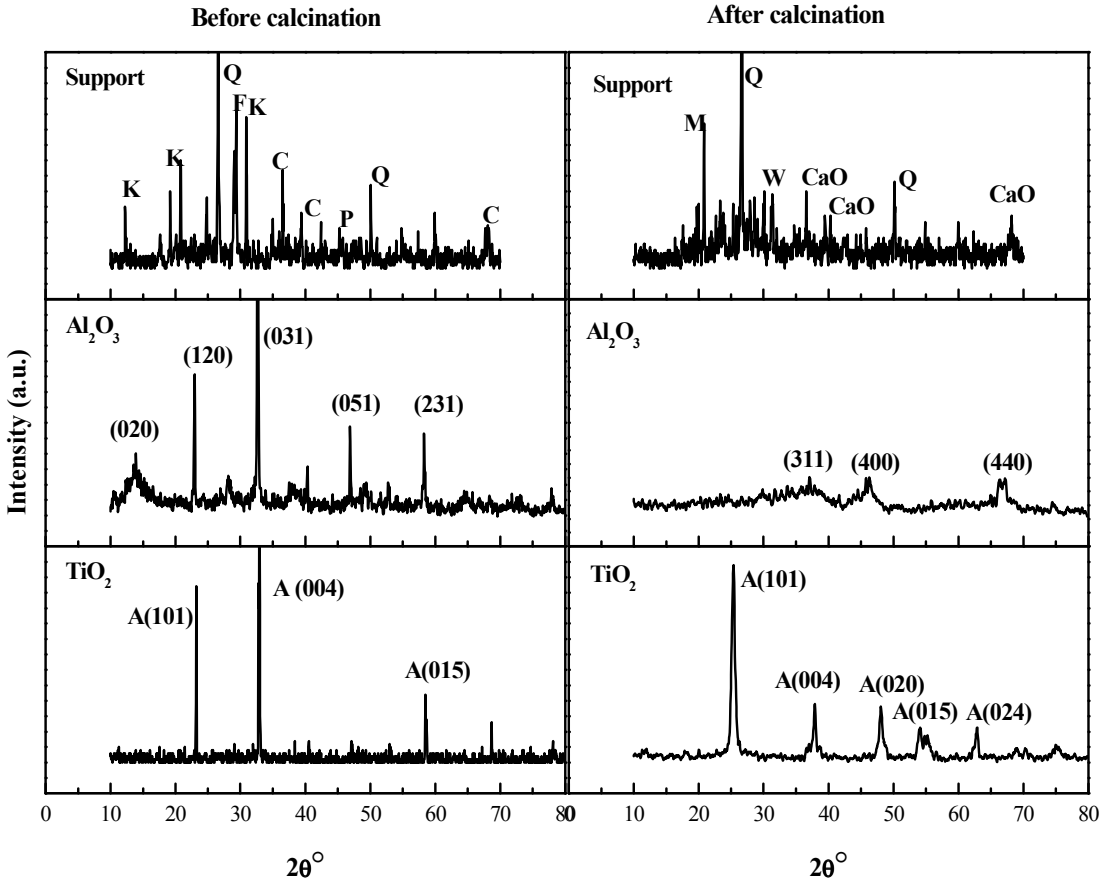


**Fig. 3** XRD profiles of the ceramic support, $TiO_2$, and $Al_2O_3$ powders before and after calcination (P-Pyrophyllite, M-Mullite, C-Calcium carbonate, F-Feldspar, CaO-Calcium oxide, W-Wollastonite, K-Kaolin and A-Anatase)

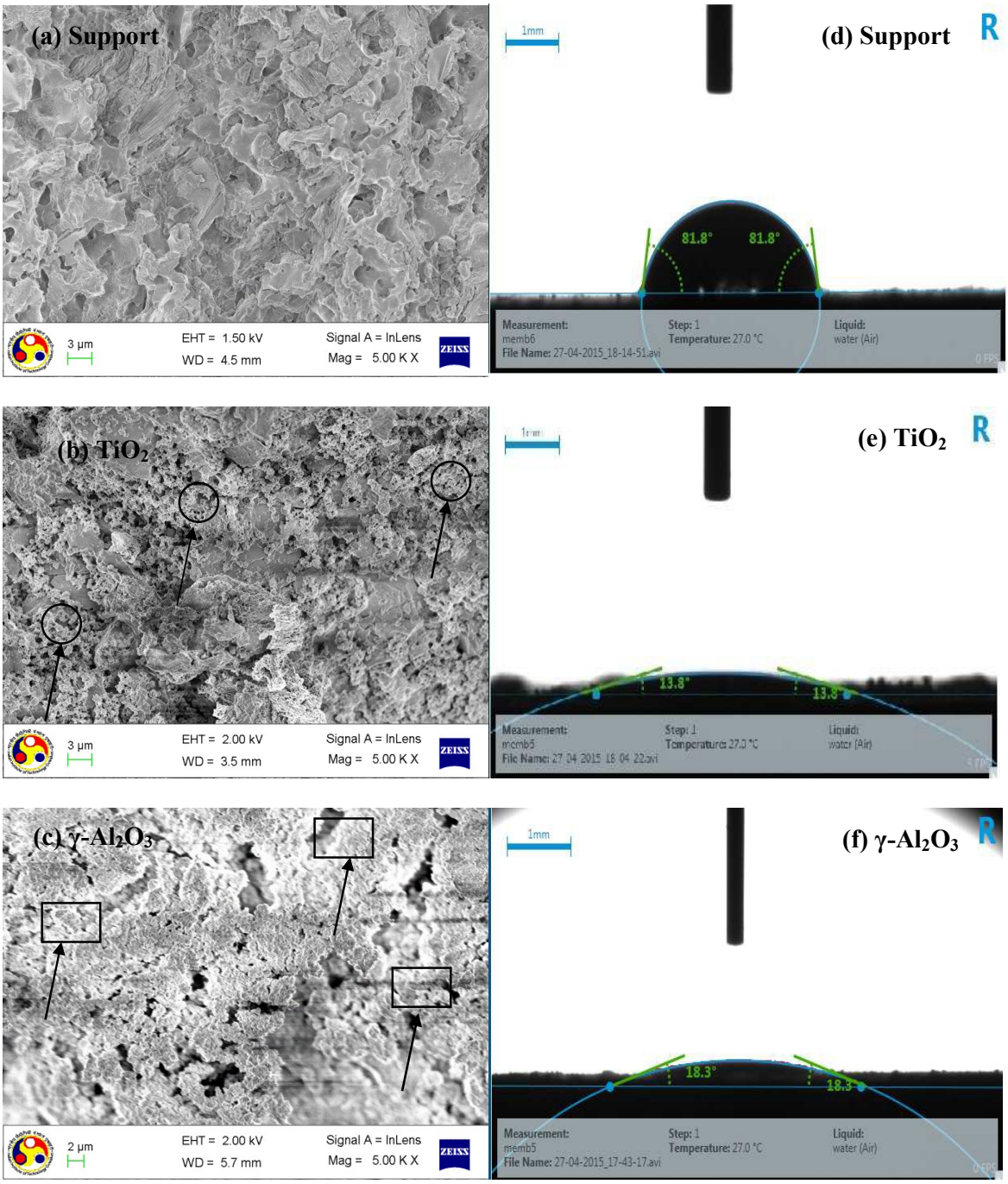


**Fig. 4** FESEM images (a,b,c) and contact angle (d,e,f) of support, $TiO_2$ and $\gamma$-$Al_2O_3$ membrane ( ◯ -$TiO_2$ layer; ▭ -$\gamma$-$Al_2O_3$ layer)

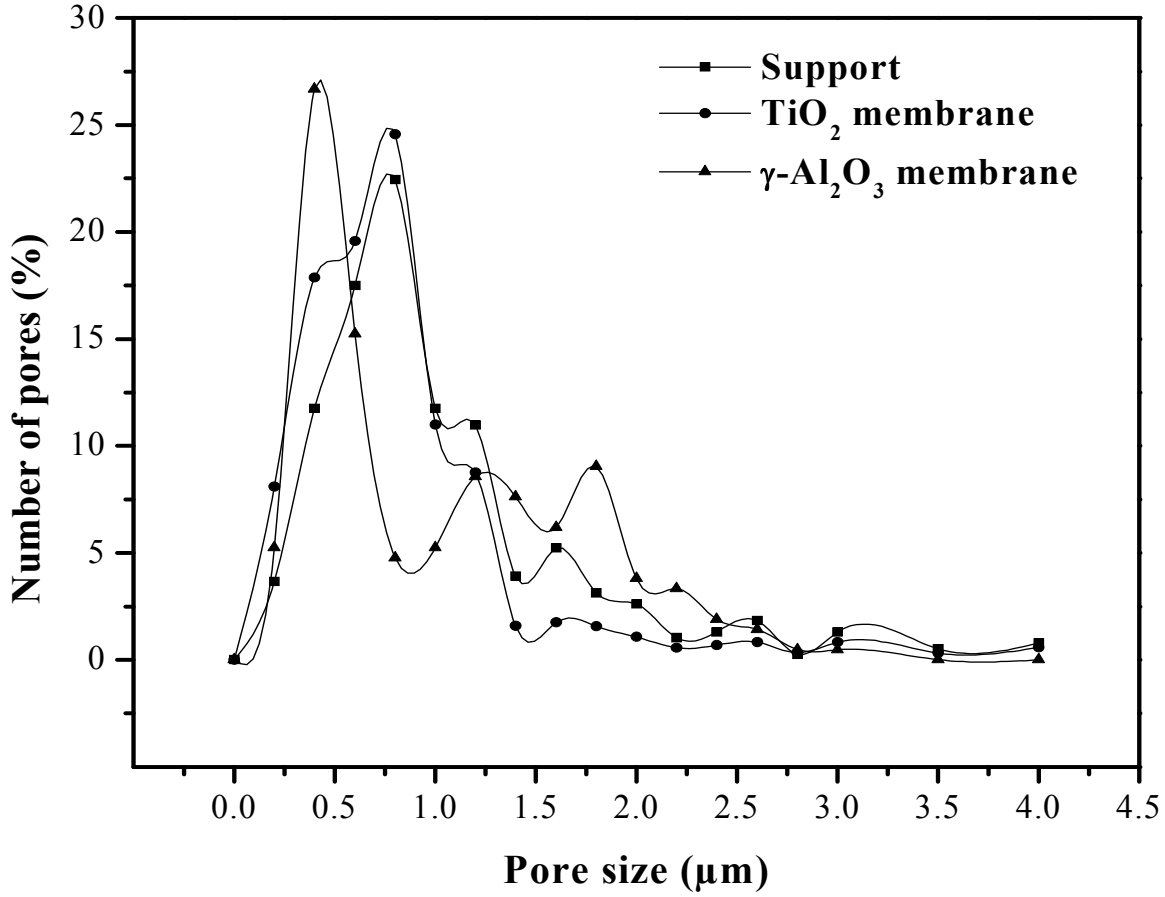


**Fig. 5** Pore size distribution of the support and membranes

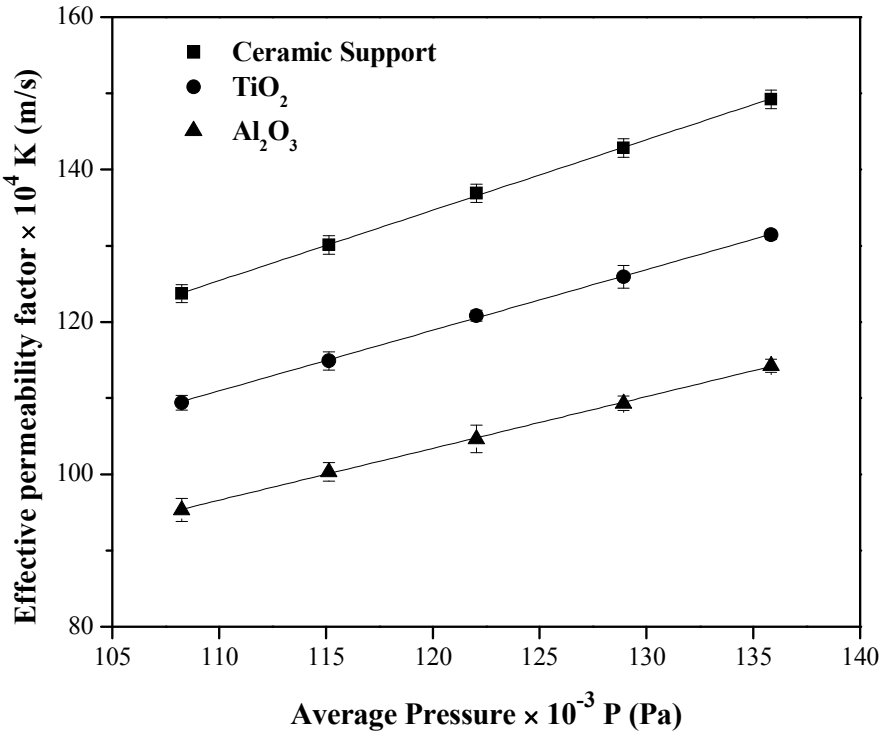


**Fig. 6** Effect of pressure on $N_2$ gas permeability of membranes and support.

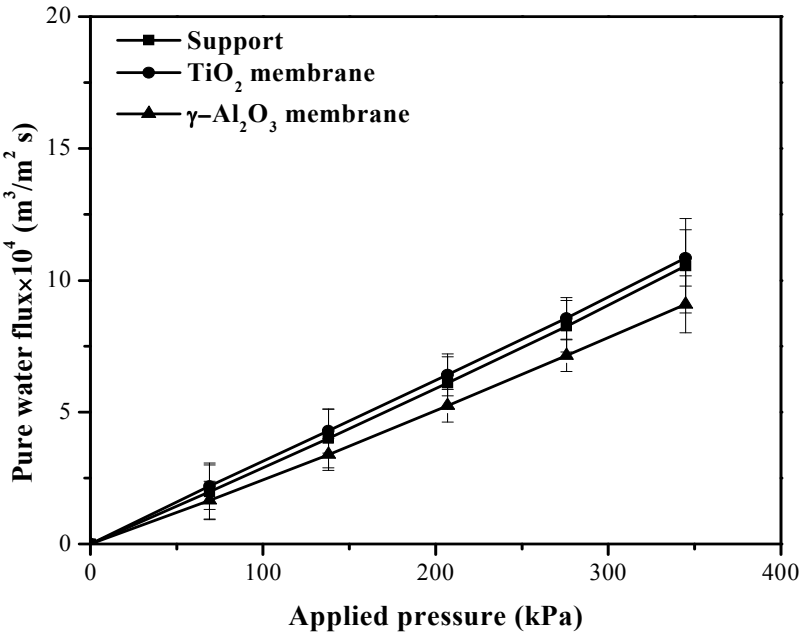


**Fig. 7** Effect of pressure on pure water flux of membranes and support.

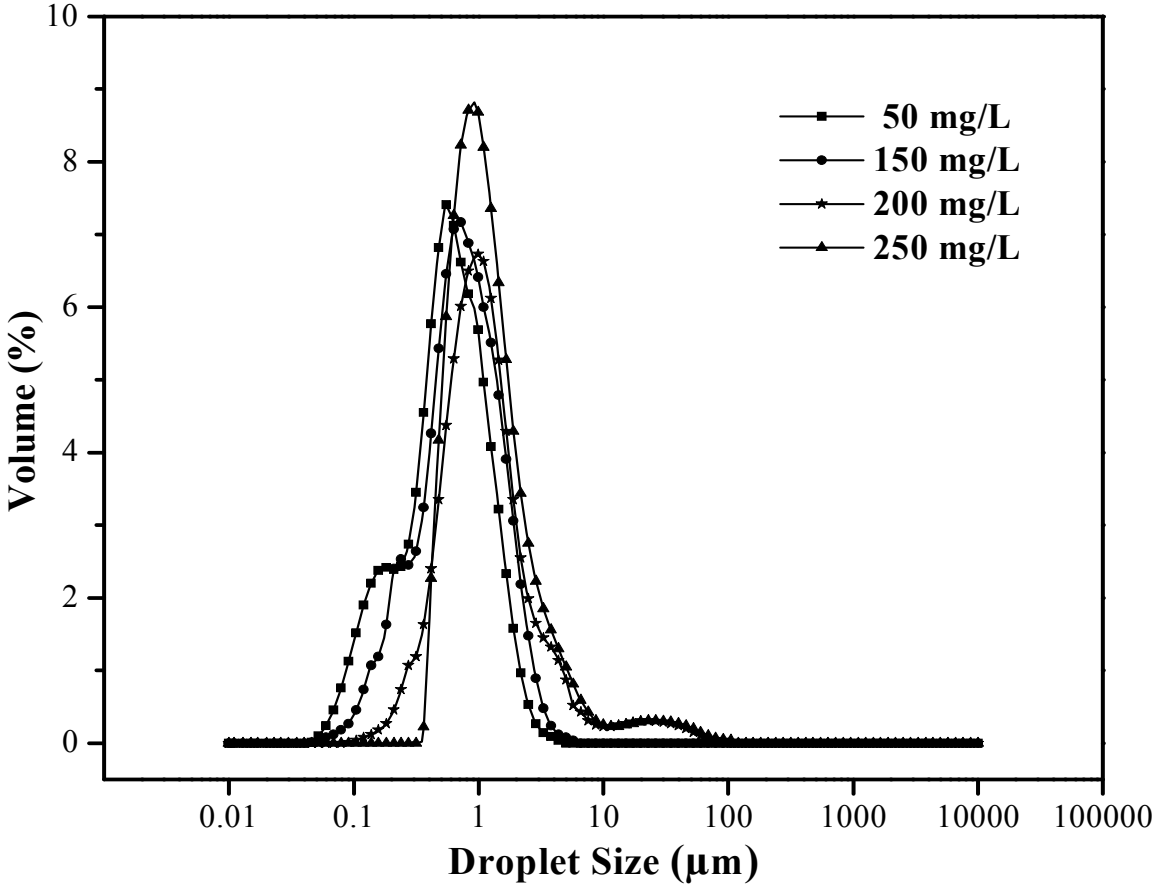


**Fig. 8** Droplet size distribution of oil-in-water emulsion

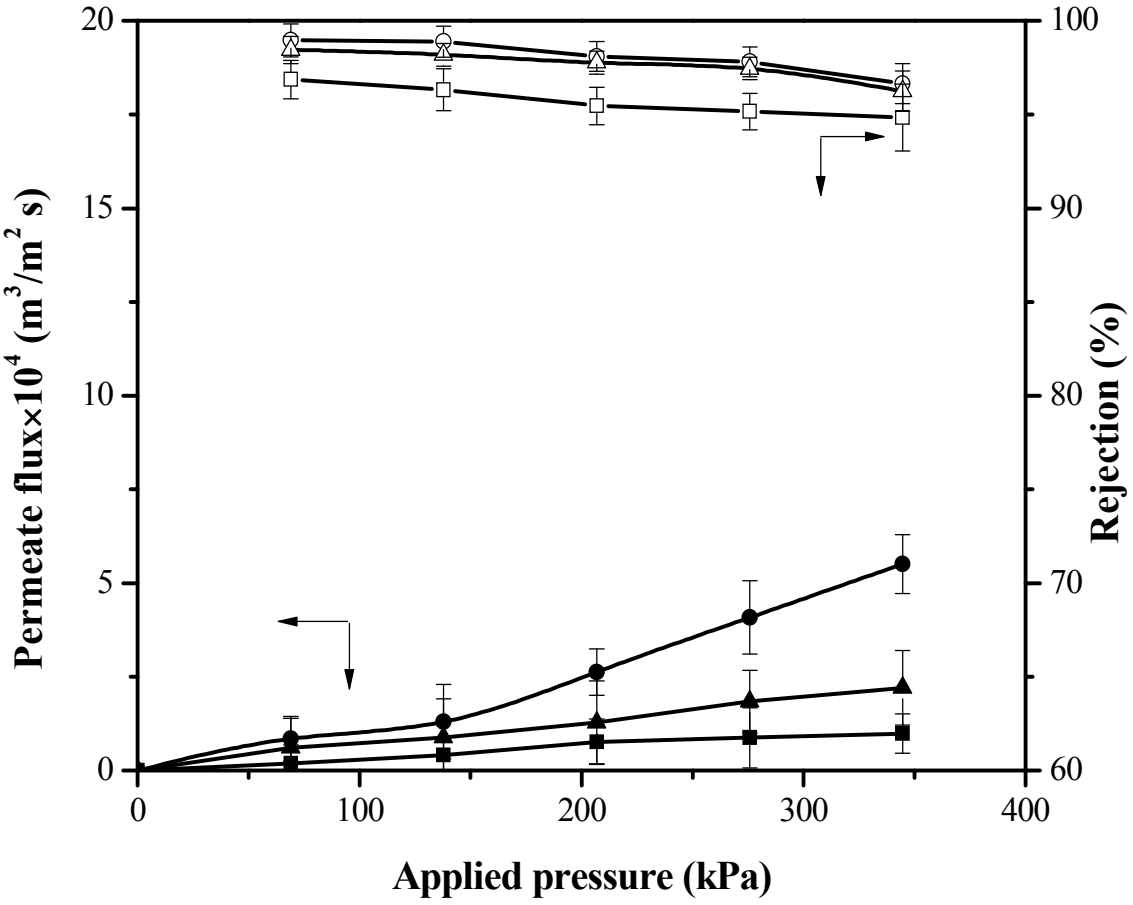


**Fig. 9** Variation of permeate flux and rejection of oil with applied pressure for support (■, □), $TiO_2$ membrane (●, ○) and γ-$Al_2O_3$ membrane (▲, Δ)

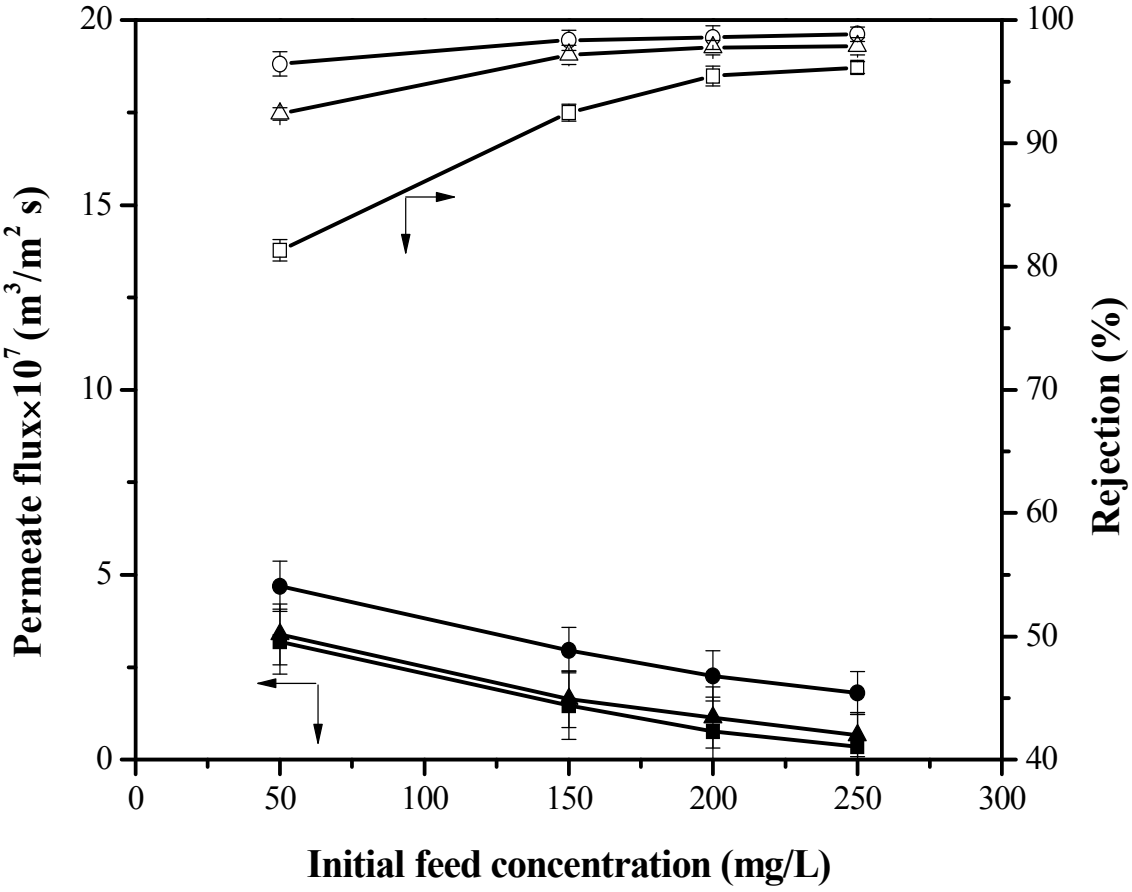


**Fig. 10** Variation of permeate flux and rejection (%) of oil with feed concentration for support (■, □), $TiO_2$ membrane (●, ○) and γ-$Al_2O_3$ membrane (▲, Δ)

**Graphical abstract:**